STRAIN FIELDS AND BENDING CRACK FAILURE ANALYSIS IN STANDARD AND THIN-RIM SPUR GEARS USING THE DIGITAL IMAGE CORRELATION METHOD

ISSN 1590-8844
Vol. 25 No. 02
2024

International Journal of Mechanics and Control

Editor: Andrea Manuello Bertetto

Scopus Indexed Journal

Reference Journal of IFToMM Italy
International Federation for the Promotion
of Mechanism and Machine Science

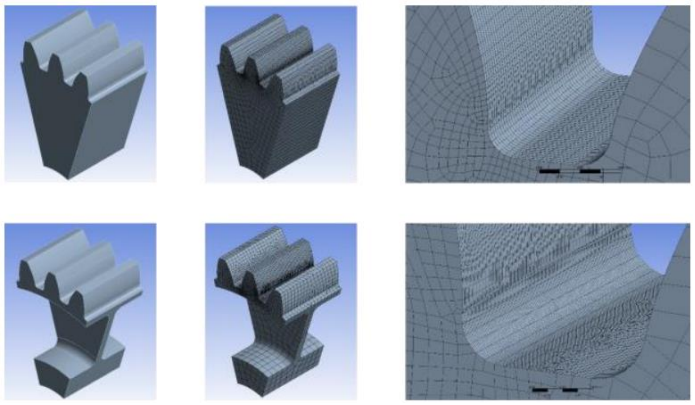

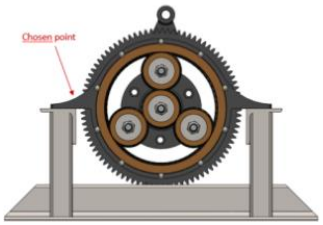

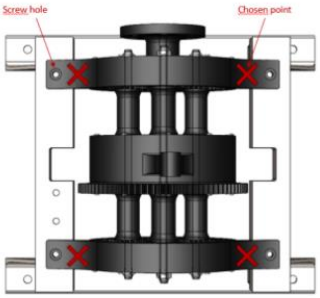

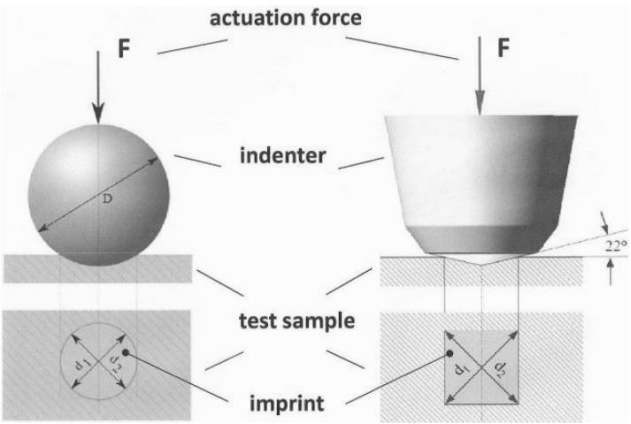

Published by ASTRA M B S.R.L.
Via Febo, 22 – 10133 – Torino (Italy)

International Journal of Mechanics and Control

Associate Editors

Published by ASTRA M B S.R.L. – Torino – Italy E.C.

Official Torino Italy Court Registration
n. 5390, 5th May 2000

Deposito presso il Tribunale di Torino
n. 5390 del 5 maggio 2000

Direttore responsabile:
Andrea Manuello Bertetto

ISSN 1590-8844
International Journal of Mechanics and Control, Vol. 25, No. 02, 2024

https://doi.org/10.69076/jomac.2024.0031

STRAIN FIELDS AND BENDING CRACK FAILURE ANALYSIS IN STANDARD AND THIN-RIM SPUR GEARS USING THE DIGITAL IMAGE CORRELATION METHOD

Francesca Maria Curà Andrea Mura Luca Corsaro

Politecnico di Torino, Department of Mechanical and Aerospace Engineering

ABSTRACT

Objective of this work is to punctually characterize the strain fields in standard and thin-rim spur gears during bending static conditions to complete and deepen a research already carried on by the authors in previous papers about the influence of gears geometry on bending crack failure. Strain profiles of two gears, standard and thin-rim respectively, were acquired and processed, so the corresponding local strain distribution was obtained. Numerical Finite Element Method simulations were run to compare and verify the corresponding experimental data. Basing on experimental and numerical obtained results, the phenomenon of the different crack propagation modes, leading to “fail safe” or “catastrophic failure”, was thoroughly analysed and interpreted.

Keywords: gears, Digital Image Correlation, numerical models, bending fatigue

1 INTRODUCTION

As well known in literature, many failures can involve gears during its operating conditions and the knowledge of related phenomena is essential to prevent them. As an example, in [1,2] authors describe many possible gear failures and how operating conditions may affect gearbox service life. In case of bending fatigue, crack propagation is one of the most critical failures in gears. The most stressed point at the tooth root zone is strictly related to the gears geometry and it influences both crack nucleation and corresponding propagation path. As also well illustrated in [3], the loading conditions play important roles in the crack initiation and propagation of metals, but further aspects such as the metals microstructure, the temperature and surrounding environmental conditions must be accurately assessed to prevent crack in metallic engineering materials.
Different crack propagation typologies may occur in gears causing generally failsafe or catastrophic failure conditions. Failsafe means that a crack may propagate through the tooth and, in this case, a failsafe design is defined, while in case of catastrophic failure the crack propagates across the wheel diameter with significant damage for the operating conditions.

Contact author: Luca Corsaro

Address: C.so Duca degli Abruzzi, 24, 10129 Torino, Italy
E-mail: luca.corsaro@polito.it

This aspect may highlight the influence of possible crack failures with design criteria, and how researchers are encouraged to study crack propagation typologies and to develop tools or devices to monitor crack growth. During the years, many studies were carried on to investigate possible crack propagation typologies in gears. Safe or catastrophic propagations and corresponding consequences for a gear with thin-rim geometry were well illustrated in [4], while in [5] the authors described how to realise an ultrasafe gear design. Crack propagation life was another parameter of interest in failsafe design. This parameter was studied in [6] on the basis of the rim thickness considering both analytical and experimental activities. The problems related to crack growth were also faced with simplified specimens similar to a spur gear tooth, as illustrated in [7]. More in detail, different surface treatments such as carburizing and shot peening were realized on these specimens to analyse their impact on crack growth. Numerical models were also developed to study fatigue failure in case of gears. As an example, a detailed analysis concerning a multiaxial fatigue approach for high-speed gears was proposed in [8]. In this study, the Finite Element Method (FEM) analysis was adopted for the evaluation of the stress tensor at the tooth root fillet considering the mesh load, the centrifugal effect and the dynamic behaviour of the gear. In [9], a numerical study on lightweight gears subjected to single tooth bending fatigue was performed to predict crack shape and crack propagation life.

Some limitations on the crack growth simulation were overcome by using a novel numerical approach, named the eXtended Finite Element Method (XFEM). It was adopted in [10, 11] to predict the crack propagation path orientation on the base of both rim dimension and initial crack position, but also in [12] to study the possible interaction between rim and web on crack propagation paths.
Rim geometry effects on fatigue crack propagation life were also studied in [13]. Authors combined the effect of different backup ratio with four drive side pressure angles. Numerical results were compared with the corresponding experimental crack propagations illustrated in [5]. A catastrophic failure occurred in case of backup ratio lower than 0.5 and an appreciable increment in the stress ratio was identified for a backup ratio of 0.3. In [14] it was also highlighted how operating conditions were relevant to realise a failsafe design. In particular, centrifugal loads due to rotational speed become a parameter of interest in crack growth evaluation and stress computation. Helical gears were also modelled with XFEM [15] to assess the crack growth and the corresponding crack under a linear elastic fracture mechanics hypothesis.
Many studies about both crack nucleation and crack growth from a mechanical point of view were developed in literature. The assumption of a mode I stress intensity factor behaviour during bending conditions was adopted in some studies ([16, 17, 18]) and results were in good accordance with numerical models or experimental campaigns designed to generate cracks on gears.
Special sensors, in addition to numerical models, were also developed to study crack nucleation and propagation from the experimental point of view. Special gauges mounted on the later faces of the gear tooth allowed to measure crack length during operating conditions. More in details, in [4] it was illustrated how the electric resistance variation may be linked to crack length in terms of number of cycles. Another example was proposed in [19], where crack propagation sensors were utilized to estimate the damage on gear tooth and to evaluate the influence of asymmetry load in crack growth.
During the recent years, Digital Image Correlation (DIC) is increasingly adopted thanks to the advantages of being a non-contact and full-field techniques and it is also suitable to observe displacement fields in small surfaces or complex components. In [20], the DIC was adopted to measure the strain field in a dynamically shear loaded aluminium specimen and experimental results were compared with FEM models. The shear strain field and principal stress vectors were analysed to predict the location of the crack even before its initiation and the corresponding crack propagation. A particular application was illustrated in [21] where DIC measured displacement of a rotating helicopter blade. Authors developed a methodology to make any rigid rotation negligible. Another potentiality of this technique was also illustrated in [22], where authors applied DIC for monitoring inhomogeneous deformation and rupture behaviour of welded joints at elevated temperature.
In this case, strain fields and ruptures were monitored during both short tensile test and for the long-term creep test. For what it concerns mechanical components as gears, the DIC was utilised to define an experimental mesh stiffness measurement for spur gears in [23]. The obtained experimental results agreed with both analytical and numerical methods.
Aim of this work was to develop an experimental approach based on the DIC technique to punctually characterize the strain fields in standard and thin-rim spur gears during bending static conditions. This analysis, verified by a corresponding numerical study, was aiming to complete and deepen a research already carried on by the authors in previous papers. In particular, measured strain profiles were related to the corresponding stress distribution in standard and thin-rim gears, strongly influenced by rim and web geometry. So, thanks to this experimental approach, results obtained in previous activities were interpreted in terms of both crack nucleation and crack growth.
Finally, the complete identification of rim and web interaction in terms of strain fields may help to prevent catastrophic failures and may provide gear's geometry recommendation in ISO Standard environment.

2 MATERIALS AND METHODS

2.1 EXPERIMENT

Two spur gears were chosen for the experimental analysis, whose geometrical parameters are resumed in Table I. In particular, depending on different backup ratio (rim dimension respect to the tooth height, mb) and web ratio (web thickness respect to the face width, mw) values, gears were identified as standard and thin-rim. Table 1 shows: pitch diameter (d), face width (b), number of teeth (z), modulus (m), backup ratio (mb), web ratio (mw) and gear blank factor (CR) [24]. Gears were made of C45 steel without thermal treatments.

Table I - Gears geometry

	Standard	Thin-rim
d [mm]	96	96
b [mm]	20	20
z	32	32
m [mm]	3	3
mb	1	0.3
mw	1	0.1
C_R	1	0.63

Gears geometry was chosen basing on results obtained by the authors [10,11,12]; in particular the thin-rim geometry, already adopted in bending fatigue tests [25], was characterized by a crack propagation path through the rim. A 3D DIC equipment (Correlated Solutions) was utilized to measure gear tooth deformations under bending static loading conditions.

In general, samples for DIC measurements have to be carefully prepared, as this operation may have a great impact on strains measurement. In this work, gears were firstly covered with a layer of white paint and then with small black speckles. An airbrush was used to better control both speckles deposition and their size.
Figure 1 shows the two samples, the standard gear on the left and the thin-rim gear on the right respectively.

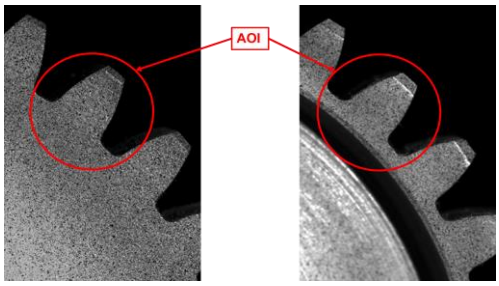

Figure 1 Samples (left, standard gear; right, thin-rim gear) and AOI.

Experimental testing acquisitions (VIC3D software) allowed to compute the deformation maps (local strain - ε_y, maximum principal strain - ε_1) and the maximum principal directions (γ_1) of each gear tooth (standard and thin-rim), referred to a chosen Area Of Interest (AOI, see Figure 1). The AOI contour was defined by a series of linear approximations and it was divided in 61 subset in order to reduce both noise level and uncertainty interval for each pixel.
DIC setup was composed of two Basler ace acA4096-30um cameras (4096x2168 pixel and sensor dimensions of 14.1x7.5 mm), one blue light source and a data acquisition unit (DAQ systems 6211). A particular equipment configuration was adopted to increase the spatial resolution. More in detail, a smart focus with two extension tubes (120mm and 24mm) and Rodagon 135 lens were mounted on each camera. Both cameras and blue light source were located on a supporting structure at 490 mm distance from the tested gear (see Figure 2, on the right).

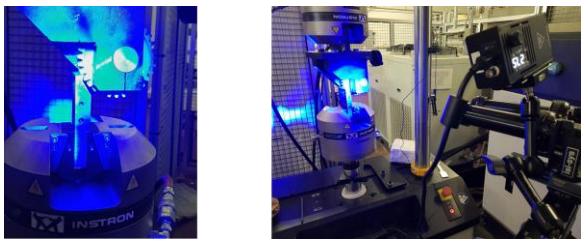

Figure 2 Experimental Setup.

A stereo angle less than 10 degrees was obtained with a distance of 25 mm between the cameras. Focus and brightness were adjusted to reduce the noise level on the images. The frame rate acquisition was 20 fps. The stereo calibration was performed with a glass target (type C) of 9*9 dots with a dot distance of 0.89mm.

The calibration results were 0.057 score for standard gear and 0.060 score for thin-rim gear. Experimental DIC setting and performance are resumed in Table 2.

Table II - Experimental DIC setting and performance

Technique used	3D Digital Image Correlation
Subset size	about 61x61 pixel^2
Step	11 pixel
Investigated area	about 9x9 mm^2
Shape function	Affine
Interpolation function	Optimazed 8-tap
Correlation criterion	Normalized squared differences
Smoothing applied to the image	Low-pass filter image
Displacement accuracy rule-of-thumb	1/100 of the field of view in-plane
Strain resolution	100 με
Differentiation method	Lagrange
Smoothing method	25 - Lagrange Method

A special device connected to a traditional tensile machine was utilized for bending tests (see Figure 2, on the left) [25], whose scheme is shown in Figure 3. An anvil integrated into the device was able to load the gear tooth along its involute profile, in both position and direction referred to the single contact point [26]. Each gear was tested at four different static loading levels, approximately: 2000 N, 4000 N, 6000 N and 8000 N.

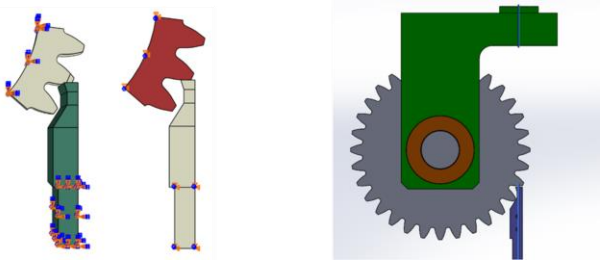

Figure 3 Special device scheme [25].

2.2 NUMERICAL MODELS

Two numerical models (standard and thin-rim gears) were developed to validate DIC results. A Static Structure Analysis with Mechanical APDL solver was implemented in Ansys Workbench Software.
Geometries with three teeth were modelled to reduce computational time for both gears, but symmetry conditions were implemented in the numerical simulation. Solid 186 elements were adopted to discretize both gear geometries (standard and thin-rim) and each model was defined with C45 steel physical (density) and mechanical (Young's modulus, yield and ultimate tensile strength) properties [27].

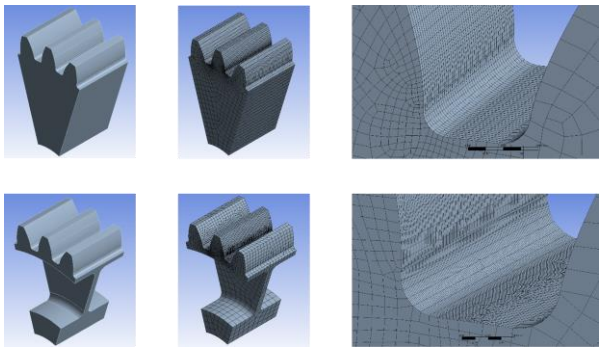

Figure 4 Standard (upper) and thin-rim (lower) model.

The equivalent stress variation was monitored to validate the optimal mesh by increasing the number of elements. Final standard and thin-rim gear models were composed by 43240 and 59384 elements respectively. Figures 4 shows both standard (upper) and thin-rim (lower) models, in particular from the left: FEM model gear geometry, whole meshed geometry, a detail of the meshed tooth root zone.

3 RESULTS

3.1 EFFECT OF RIM AND WEB INTERACTION ON CRACK INITIATION AND PROPAGATION

Preliminary numerical analysis with XFEM models were performed to investigate bending crack failures in thin-rim spur gears during bending conditions [12]. Different geometries were considered to study the effect of rim and web interaction on the crack initiation point and the corresponding propagation. Figure 5 illustrates the obtained numerical results.

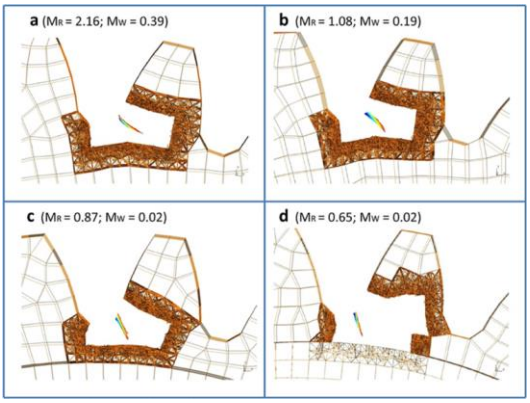

Figure 5 Numerical crack propagation paths [12].

Figure 5 showed different possible crack propagation paths (failsafe, a; catastrophic failure, b-c-d) as a function of the gear's geometry (MW= mw, see Table 1; MR is [12] the rim dimension respect to the normal modulus, similar to the backup ratio mb). A safe zone was defined for web ratio (MW) higher than 0.2 and for a rim ratio (MR) higher than 2.16, according to ISO 6336 Standard [24]. Two similar gears (same material and geometry) were chosen to validate these numerical results with fatigue tests, where the surface thermal profile was monitored by an IR thermocamera [25].

Figure 6 Failures on standard (left side) and thin-rim (right side) gears subjected to fatigue tests [25].

Figure 6 shows both gears (standard and thin-rim) tested under bending fatigue condition up to failure.
In particular, Figure 6 shows two different failures, respectively through the tooth and through the rim, obtained in standard (left side) and thin-rim (mb= 0.3, MR =0.65, mw=0.1) (right side) gears. A Scanning Electron Microscope (SEM) image referred to one of the tested teeth may be observed in Figure 7. It allows to validate the hypothesis, utilized in numerical XFEM models [12, 14, 25], of modelling a crack with an elliptic shape close to the most stressed point.

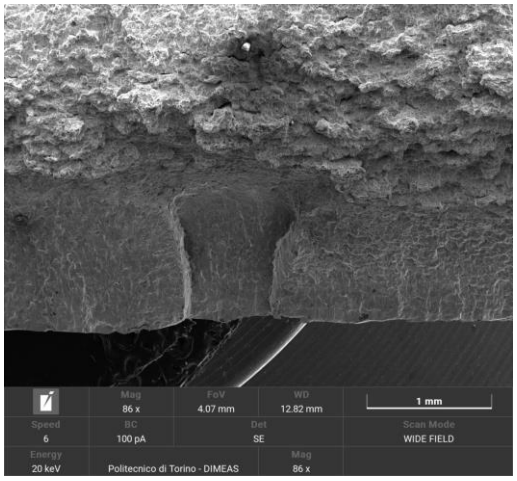

Figure 7 SEM image of an elliptical defect.

Same geometry and material for gears were adopted in this work for the experimental characterisation based on the DIC technique. The analysis aimed to describe in a complete way the strain field on each gear and the obtained results were related to failsafe and catastrophic failures.

3.2 DIC AND FEM RESULTS

In this section, both experimental and numerical results are illustrated. For sake of brevity, only results related to the maximum loading value are presented.
A local reference system was defined for both standard and thin-rim gears, shown respectively in Figures 8. More in detail, the y-axis corresponds to the tooth centreline and the x-axis position refers to the tooth root.
Figure 9 shows the local reference system and the position of three lines (Line 0, 1, 2), parallel to the x-axis, whose y-position was defined in the tooth root zone for data post processing (VIC3D environment).

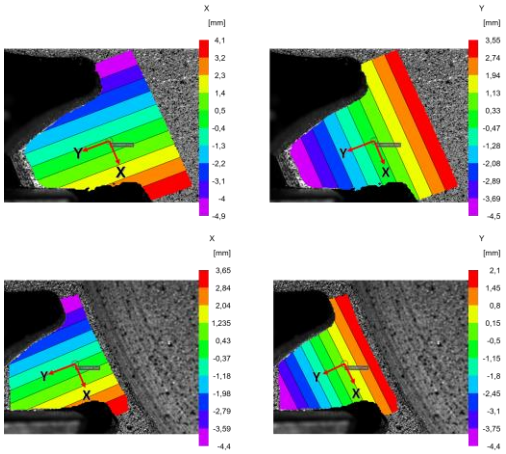

Figure 8 Local reference system for standard (upper) and thin-rim (lower) gears.

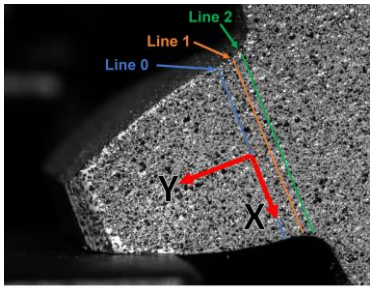

Figure 9 Lines location on the tooth root and local reference system for standard gear.

Experimental local strain profiles ε_y were extracted from deformation maps and along these lines (Line 0, 1, 2). More in detail, Line 0 was located at the centre of the local reference system (y = 0, initial point of the tooth root fillet), Line 1 at -0.5 mm (y = -0.5 mm, corresponding to the points at which the 30° tangents are in contact with the root fillets (for external gears)) and Line 2 at -0.75 mm (y = -0.75 mm) from the centre of the local reference system [25]. Figure 10 show respectively experimental (upper) and numerical (lower) local strain profiles ε_y, extracted from Lines 0, 1, 2, for standard (on the left) and thin-rim (on the right) gears. All graphs point out a good agreement between experimental and numerical results and allow to interpret and verify the classical bending behaviour of gears described in literature [26, 28]. In particular, the standard gear generates, at the tooth root fillet, a local strain profile ε_y congruent to the beam theory, including the notch effect. On contrary, the thin-rim gear shows a different bending behaviour, above all in its central zone, emphasising a possible tooth rotation due the flexibility of the rim and web [24]. This phenomenon may be also observed representing the normalized experimental and numerical local strain profiles ε_y at the Line 0 for the two gears, computed with respect to the maximum positive value of each gear (see Figure 11).

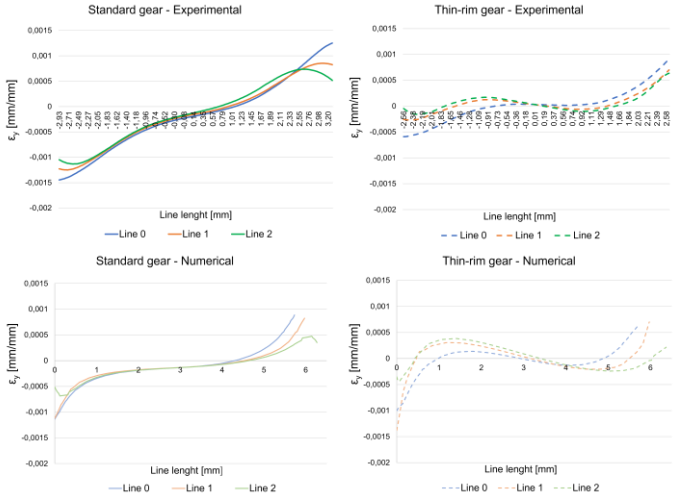

Figure 10 Experimental and numerical local strain profiles ε_y.

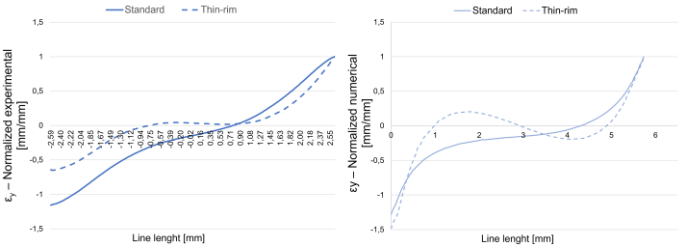

Figure 11 Normalized experimental (on the left) and numerical (on the right) local strain profiles ε_y.

Standard and thin-rim gears show a substantial different behaviour not only for as concerns ε_y strain profiles at the tooth root, but also referring to equivalent and principal stress and strain maps.
In general, bending crack propagation starts from the most stressed point (maximum equivalent stress value) and follows different paths, through the tooth or through the rim respectively [4, 5, 11, 12, 14].

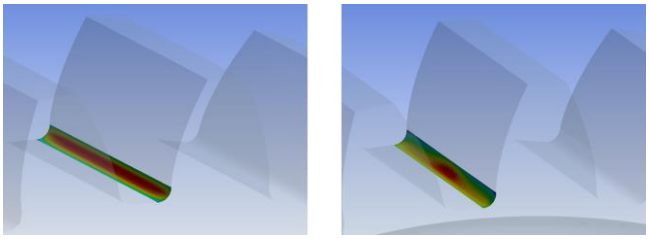

Figure 12 Calculated maximum strain ε_1 values and position along the face width.

Also in axial direction, along the face width, the different geometry of gears strongly influences the principal strain maps, as qualitatively shown in Figure 12; maximum principal strain values ε_1 are here represented by a red distribution in the tooth root fillet zone.

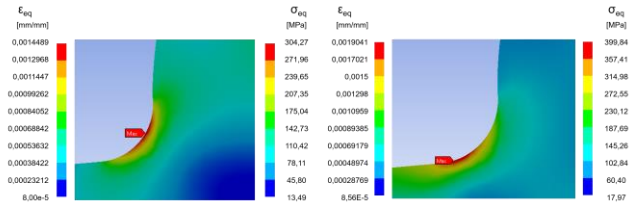

Figure 13 Calculated maximum equivalent stress σ_{eq} and strain values ε_{eq} and position (left side for standard gear and right side for thin-rim gear).

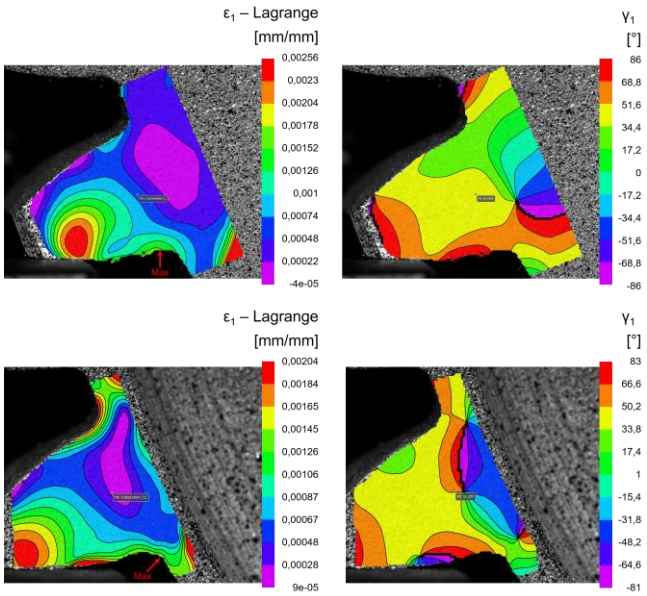

Figure 14 Experimental maximum principal strain ε_1 and maximum principal direction γ_1 maps for standard (upper) and thin-rim (lower) gears.

Figure 13 shows the calculated maximum equivalent stress σ_{eq} and strain ε_{eq} values, with the corresponding position on the tooth root fillet for both gears. Maximum principal strain ε_1 profiles, starting from the most stressed point, may represent a good parameter to compare the bending behaviour of standard and thin-rim gears, as shown in Figure 11. More in detail, the upper part of Figure 14 illustrates experimental DIC results in terms of maximum principal strain ε_1 and maximum principal direction γ_1 maps for the standard gear. The lower part of Figure 14 shows the corresponding maps for the thin-rim gear.

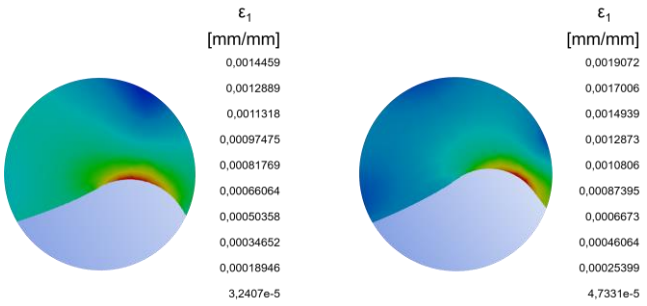

Figure 15 Numerical maximum principal strain ε_1 for standard (left side) and thin-rim (right side) gears.

Furthermore, Figure 15 shows in detail the numerical maximum principal strain profile ε1 and its position calculated at the tooth root fillet for standard (left side) and thin-rim (right side) gears.

4 DISCUSSION

From the analysis of all results, it can be observed that standard and thin-rim gears present different behaviours from strains and stresses point of view. As an example, ε_1 and γ_1 maps (Figure 14) were substantially different, above all in both tooth root fillet and rim zones. In particular, the maximum value of maximum principal strain maps ε_1 was measured close to the tooth root fillet for the standard gear, while the corresponding maximum value for the thin-rim gear was obtained as shifted through the rim. It may be also observed that, for both standard and thin-rim gears, the loading application zone emphasised a high stress (and strain) condition. Numerical maximum principal strains ε_1 (Figure 15) substantially matched experimental results in both tooth root fillet and rim zones.

These results allow to interpret the different crack propagation peculiarities ("fail safe" and "catastrophic failure") when a bending damage occurs.

Maximum principal direction γ_1 maps of standard and thin-rim gears (Figures 14) may be interpreted in the same way, emphasizing different changes in direction along the tooth root. In particular, a discontinuity of the maximum principal direction may be depicted near the maximum principal strain ε_1 at the tooth root and, as a consequence of that, near the crack starting point. Maximum principal direction γ_1 maps also pointed out a strong difference in the bending behaviour of gears in their central zone, as already shown by graphs of Figure 11.

This way, the effect of rim and web on the maximum principal strain maps ε_1 is highlighted. The interaction between geometrical parameters, maximum principal strain maps ε_1, and corresponding crack nucleation and crack propagation, is related to the gear's flexibility, well represented by ISO gear blank factor CR [24]. As a matter of fact, to prevent crack propagation through the rim, gear's geometry has to be properly chosen according to the safe zone of gear blank factor CR [24].

5 CONCLUSIONS

This research activity was carried on in order to provide a deeper interpretation of the phenomenon of different crack propagation paths in gears under bending conditions, leading to "fail safe" or "catastrophic failure".

To this aim, an experimental approach based on the DIC technique to punctually characterize the strain fields was developed, parallel to a corresponding numerical FEM analysis. For both experimental and numerical analysis standard and thin-rim gears were adopted, whose geometry was properly chosen.

Basing on obtained results, the following conclusions may be drawn.

DIC technique, despite the difficulties in set up and calibration, may be considered as a useful methodology to provide local and global measurements of strain maps. In particular, it may be observed that principal strain maps may represent a good parameter to monitor the bending behaviour of gears whose geometry is responsible for the corresponding fracture typology. This aspect was confirmed by numerical simulations. Basing also on previous research activities, it may be observed that the crack initiation phenomenon, related to the most stressed point at the tooth root, may now be interpreted and deeper explained. This work allows the designers to consider a different point of view, emphasising the necessity of taking into account all strain fields in addition to equivalent strain and stress values, above all for thin-rim gears.
Finally, it can be concluded that the strain fields knowledge may be generally represent a valid help in designing thin-rim gears, focusing on a rim and web geometry that corresponds to a blank factor value referred to the uncertainty zone for as concerns the crack propagation path.

REFERENCES

[1] Maláková S., Sivák S., Fedorko G., Molnár V. and Tomek M., Analysis of damage origin of bevel gear wheels, *Engineering Failure Analysis*, Vol. 146, 2023.

[2] Ristivojević M., Lučanin V., Dimić A., Mišković Ž., Burzić Z., Stamenić M. and Rackov M., Investigation of the heavy duty truck gear drive failure, *Engineering Failure Analysis*, Vol. 144 (106995), 2023.

[3] Hoang V. T., The mechanism of crack initiation and propagation in metallic engineering materials, *International Journal of Mechanics and Control*, Vol. 15 (2), 2014.

[4] Lewicki D. G., *Crack propagation studies to determine benign or catastrophic failure modes for aerospace thin-rim gears*, NASA Technical Memorandum 107170, 1996.

[5] Lewicki D. G., *Gear Crack propagation path studies, guidelines for ultra-safe design*, NASA Technical Memorandum 211073, 2001.

[6] Lewicki D.G. and Ballarini R., Rim Thickness Effects on Gear Crack Propagation Life, *International Journal of Fracture*, Vol. 87, pp. 59-86, 1997.

[7] Blarasin A., Guagliano M. and Vergani L., Fatigue crack growth prediction in specimen similar to spur gear teeth, *Fatigue & Fracture of Engineering Materials & Structures*, Vol. 20, pp. 1171-1182, 1997.

[8] Curà F., Gallo F, Rosso C., A study of fatigue in high speed gears, *International Journal of Mechanics and Control*, Vol 14 (2), 2013.

[9] Lewicki D. G., *Three-Dimensional Gear Crack Propagation Studies*, NASA Technical Memorandum -208827, 1998.

[10] Curà F., Mura A. and Rosso C., Investigation about crack propagation paths in thin rim gears, *Fracture and Structural Integrity*, Vol. 30, pp. 446-453, 2014.

[11] Curà F., Mura A. and Rosso C., Crack propagation behaviour in planet gears, *Procedia structural integrity*, Vol. 2, pp. 3610-3616, 2016.

[12] Curà F., Mura A. and Rosso C., Effect of rim and web interaction on crack propagation paths in gears by means of XFEM technique, *Fatigue & Fracture of Engineering Materials & Structures*, Vol. 38, pp. 1237-1245, 2015.

[13] Oğuz D., Celalettin Y. and Fatih K., Effects of Rim Thickness and Drive Side Pressure Angle on Gear Tooth Root Stress and Fatigue Crack Propagation Life, *Engineering Failure Analysis*, Vol. 122 (105260), 2021.

[14] Curà F., Mura A. and Rosso C., Influence of high speed on crack propagation path in thin rim gears, *Fatigue & Fracture of Engineering Materials & Structures*, Vol. 40, pp. 120-129, 2017.

[15] Amiri Rad A., Forouzan M.R. and Sadeghi Dolatabadi A., Three-dimensional fatigue crack growth modelling in a helical gear using extended finite element method, *Fatigue & Fracture of Engineering Materials & Structures*, Vol. 37, pp. 581-591, 2014.

[16] Guagliano M. and Vergani L., Mode I stress intensity factors for curved cracks in gears by a weight functions method, *Fatigue & Fracture of Engineering Materials & Structures*, Vol. 24, pp. 41-52, 2001.

[17] Guagliano M. and Vergani L., Effect of crack closure on gear crack propagation, *International Journal of Fatigue*, Vol. 23, pp. 65-73, 2001.

[18] Zhang X., Li L., Qi X., Zheng J., Zhang X., Chen B., Feng J. and Duan S., Experimental and numerical investigation of fatigue crack growth in the cracked gear tooth, *Fatigue & Fracture of Engineering Materials & Structures*, Vol. 40, pp. 1037-1047, 2017.

[19] Nenadic N. G., Ardis P. A., Hood A. A., Thurston M. G. and Lewicki D. G., Processing and interpretation of crack-propagation sensors, *Proc. of annual conference of the prognostics and health management society, PHM Society*, pp. 560-568, 2015.

[20] Litrop A., Zobec P., Šeruga D., Nagode M. and Klemenc J., Experimental analysis of crack initiation and propagation in dynamically shear-loaded aluminium specimens using the digital image correlation method, *Engineering Failure Analysis*, Vol. 139 (106495), 2022.

[21] Sousa P. J., Barros F. and Tavares P. J. and Moreira P. M.G.P., Digital image correlation displacement measurement of a rotating RC helicopter blade, *Engineering Failure Analysis*, Vol. 90, pp. 371-379, 2018.

[22] Song M., Sun C., Zhang X., Yu H., Sun Y., Liu K. and Xu T., The test on the inhomogeneous strain field and creep rupture behavior of the weld joint at elevated temperature by digital image correlation method, *Engineering Failure Analysis*, Vol. 120 (104997), 2021.

[23] Raghuwanshi N. K. and Parey A., Experimental measurement of spur gear mesh stiffness using digital image correlation technique, *Measurement*, Vol. 111, pp. 93-104, 2017.

[24] International Standard Organization, *Standard ISO 6336 - Part1: Calculation of Load Capacity of Spur and Helical Gears*, 2019.

[25] Curà F., Mura A. and Corsaro L., Experimental investigation on crack propagation paths in spur gears, *IOP Conf. Series: Materials Science and Engineering*, Vol. 1214 (012029), 2022.

[26] International Standard Organization, *Standard ISO 6336 - Part3: Calculation of Load Capacity of Spur and Helical Gears*, 2019.

[27] Matière du monde, *Acier C45 FicheTechnique, Matière 1.0503 Caractéristiques Mécaniques*. https://matieredumonde.com/acier-c45/#Acier_C45_Caracteristiques_Mecaniques (accessed 15 June 2022).

[28] Budynas R.G. and Nisbett J.K., *Shigley's Mechanical Engineering Design*, McGrow-Hill Education, 2021.

International Journal of Mechanics and Control – JoMaC
Published by ASTRA M B S.R.L.

TRANSFER OF COPYRIGHT AGREEMENT

NOTE: Authors/copyright holders are asked to complete this form signing section A, B or C and mail it to the editor office with the manuscript or as soon afterwards as possible.	*Editorial Secretary address:* Andrea Manuello Bertetto Matteo D. L. Dalla Vedova, Simone Venturini, Alessandro Aimasso *Dept. of Mechanical and Aerospace Engineering* *Politecnico di Torino* *C.so Duca degli Abruzzi, 24 – 10129 Torino – Italy* *e_mail: jomac@polito.it* *fax n.: +39.011.090.6999*

The article title:

By:_____

To be Published in ***International Journal of Mechanics and Control JoMaC***
Official legal Turin court registration Number 5320 (5 May 2000) - reg. Tribunale di Torino N. 5390 del 5 maggio 2000

A Copyright to the above article is hereby transferred to the JoMaC, effective upon acceptance for publication. However the following rights are reserved by the author(s)/copyright holder(s):
1. All proprietary rights other than copyright, such as patent rights;
2. The right to use, free or charge, all or part of this article in future works of their own, such as books and lectures;
3. The right to reproduce the article for their own purposes provided the copies are not offered for sale.

To be signed below by all authors or, if signed by only one author on behalf of all co-authors, the statement A2 below must be signed.

A1. All authors:

SIGNATURE_____DATE_____ SIGNATURE_____DATE_____

PRINTED NAME_____ PRINTED NAME_____

SIGNATURE_____DATE_____ SIGNATURE_____DATE_____

PRINTED NAME_____ PRINTED NAME_____

A2. One author on behalf of all co-authors:
"I represent and warrant that I am authorised to execute this transfer of copyright on behalf of all the authors of the article referred to above"

PRINTED NAME_____

SIGNATURE_____ TITLE_____ DATE_____

B. The above article was written as part of duties as an employee or otherwise as a work made for hire. As an authorised representative of the employer or other proprietor. I hereby transfer copyright to the above article to *International Journal of Mechanics and Control* effective upon publication. However, the following rights are reserved:
1. All proprietary rights other than copyright, such as patent rights;
2. The right to use, free or charge, all or part of this article in future works of their own, such as books and lectures;
3. The right to reproduce the article for their own purposes provided the copies are not offered for sale.

PRINTED NAME_____

SIGNATURE_____ TITLE_____ DATE_____

C. I certify that the above article has been written in the course of employment by the United States Government so that no copyright exists, or by the United Kingdom Government (Crown Copyright), thus there is no transfer of copyright.

PRINTED NAME_____

SIGNATURE_____ TITLE_____ DATE_____

CONTENTS - Special Issue of the International Journal of Mechanics and Control (JoMaC) dedicated to the 6th International Tunisian Conf. on Mechanics (COTUME 2023)

CONTENTS – Regular Issue

NEWS FROM THE JOMAC EDITORIAL BOARD:

Starting from the June 2024 issue, JoMaC provides an Open Access service to our authors. You are invited to visit the JoMaC website (http://www.jomac.it) for further details.